Experimental evaluation at pilot plant scale of multiple PCMs (cascaded) vs. single PCM configuration for thermal energy storage

Gerard Peiró, Jaume Gasia, Laia Miró, Luisa F. Cabeza

GREA Innovació Concurrent, Universitat de Lleida, Edifici CREA, Pere de Cabrera s/n, 25001, Lleida, Spain. Tel: +34.973.00.35.77. Email: lcabeza@diei.udl.cat

Abstract

The present paper provides on one hand, a literature review of the different studies available in the scientific literature where the concept of multiple phase change materials (PCM) configuration, also named cascaded or multi-stage, has been presented and on the other hand, an experimental evaluation of the advantages of using the multiple PCM configuration instead of the single PCM configuration in thermal energy storage (TES) systems at pilot plant to fill the gap of experimental and high scales studies on this concept in the literature. Two PCM with melting temperatures in a temperature range of 150-200 ºC were selected due to their high value of heat of fusion and compared: d-mannitol and hydroquinone. Three configurations were evaluated: (1) single PCM with hydroquinone, (2) single PCM with d-mannitol and (3) multiple PCM with hydroquinone and d-mannitol. A discussion regarding the results on the specific energy stored and effectiveness as well as the evolution of the PCM and heat transfer fluid (HTF) through the time and at different and representative locations of the facility is presented. Results showed that the multiple PCMs configuration introduced an effectiveness enhancement of 19.36 % if compared with single PCM configuration as well as a higher uniformity on the HTF temperature difference between the inlet and outlet.

Keywords:

Thermal energy storage, phase change material, thermal performance enhancement, multiple PCM, cascaded

Nomenclature

A	Heat exchanger surface, m^2
D	Diameter, m
DMA	D-mannitol
f	Friction factor, -

h	Enthalpy, J/kg·K
H	Melting enthalpy, J/kg
HTF	Heat transfer fluid
HYD	Hydroquinone
k	Thermal conductivity, W/m·K
L	Average pipe length, m
Nu	Nusselt dimensionless number, -
PCM	Phase change material
Pr	Prandtl dimensionless number, -
$\dot{Q}$	Heat transfer rate, W
R	Thermal resistance, K/W
Re	Reynolds dimensionless number, -
S	Shape factor, m
T	Temperature, ºC
U	Global heat transfer coefficient, W/m^2·K
W	Distance between pipes, m
%wt	Weight percent

Greek symbols

Δh	Variation of enthalpy, J/kg·K
ΔT	Variation of temperature, ºC
α	Convective heat transfer coefficient, W/m^2·K
ε	Effectiveness
μ	Fluid viscosity, Pa·s

Subscripts

b	Bulk
eff	Effective
ext	External
f	Final
i	Initial
in	Inlet
int	Internal
LMTD	Logarithmic mean temperature difference
m	Melting
mid	Middle

n	PCM number n
out	Outlet
p	Pipe
t	Total
w	Pipe wall

1. Introduction

Nowadays practically all the countries base their energetic model in the exploitation of fossil fuels, but this model cannot be maintained indefinitely due to the danger for both the environment and the humanity. In fact, the International Energy Agency (IEA) [1] is now focused on the affordability, sustainability and reliability of the global energy system. Hence it is necessary to develop energy alternatives such as thermal energy storage (TES).

Among the possible TES options, multiple PCMs configuration, also called by some researchers as cascaded or multistage configuration, is a TES system design where different types of phase change materials (PCM) with different melting temperatures and enthalpies are arranged in series in order to enhance the overall heat transfer performance of the system. This configuration aims to increase low storage capacities in the single PCM due to the poor PCM thermal conductivities. As it can be observed in Fig. 1, the most suitable arrangement of a multiple PCM system is obtained by placing the PCMs in a decreasing order of their melting temperatures and moreover in an increasing order of their melting enthalpies in the heat transfer fluid (HTF) flow direction during the charging process, and the other way around during the discharging process [2]. Therefore, in order to achieve the greatest performance improvement, researchers need to study the properties of the candidate materials with the aim of not selecting them arbitrarily but select the suitable combination and with the proper dimensions for the desired application.

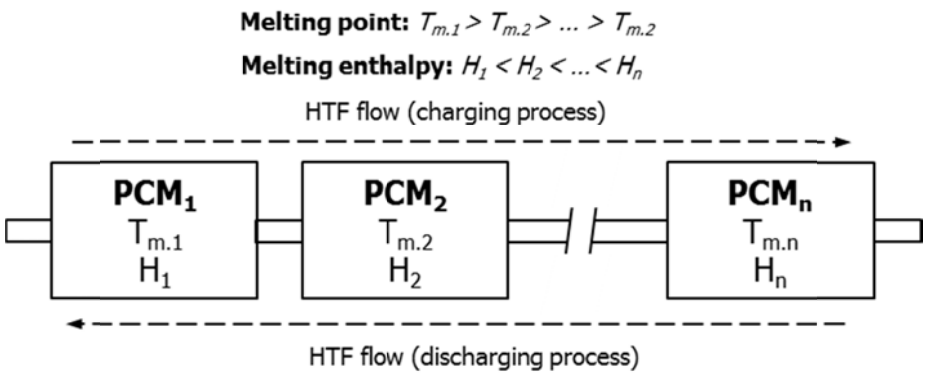

Fig. 1. Suitable multiple PCMs configuration for "n" PCMs considering their melting temperature (T_m) and the melting enthalpy (H).

The following advantages of the use of multiple PCMs configuration have been numerically and experimentally proven in previous studies:

- Increase in the heat transfer rate during charging and discharging, especially when change of phase is occurring [3-6]. The heat transfer rate in a TES system depends on the temperature difference between the HTF and the PCM. If these PCMs are arranged in a decreasing order of their melting points, then nearly a constant temperature difference can be maintained along the flow direction during all the process and therefore a more uniform heat transfer rate. On the other hand, if a single PCM configuration is used, the temperature difference between the PCM and the HTF decreases along the flow direction and therefore a heat transfer rate with a decreasing tendency is obtained. Farid and Kanzawa quantified numerically [7] and experimentally [8] an increase up to 10% and 15 %, respectively in the latent heat period. Moreover, this increase of the heat rate can lead to a volume and mass decrease of the storage system and consequently the economical investment [9].
- Uniform and lower outlet HTF temperature for a longer period during the charging and discharging process [7,10,11]. Solar based thermal power plants [3] and solar heat receivers [9] can benefit from this nearly isothermal working fluid conditions.
- Faster charging and discharging processes [4]. Chiu and Martin [12] accounted for 20% and 40% of reduction in the discharging and charging time, respectively and Seeniraj and Lakshmi Narasimhan [3] found that the amount of melted fraction in the same period of time increased in multiple PCM configurations.
- Increase of exergy efficiency by reducing the exergy losses of the system [4,5,13].

However, most of these advantages are only proven by numerical studies. Moreover, in the few experimental cases available in the literature [4,7,10] less advantages than expected are found due to the limitation of the modelling tools and the way that PCMs are considered (as a pure material, implying a single melting temperature instead a melting temperature range).

In the present paper, the experimental performance at pilot plant scale of a multiple PCMs system using hydroquinone and d-mannitol is shown, representing the highest experimental scale studied until this moment. Moreover, this work scale allows a detailed study of the temperatures in several and representative locations of the facility. Melting temperatures of the studied PCMs make them suitable in such diverse applications as solar refrigeration systems

coupled with concentrating solar collectors [14] and industrial waste heat recovery systems [15]. The advantages of using multiple PCMs configuration systems versus using single PCM configuration storage system are expected to be shown in this study when regarding the following parameters over the time: PCM and HTF temperatures profiles of the TES tank, energy stored per unit of mass and effectiveness.

2. Materials and methodology

2.1 Phase change materials

The PCMs studied were hydroquinone, commercialized by QUIMIVITA with a purity of 95 %wt, and d-mannitol, commercialized by QUIMIVITA with a purity of 96 %wt and characterized as δ-phase. In this study the melting temperature of each material and the melting enthalpy were obtained with differential scanning calorimeter (DSC) analysis. The equipment used to obtain these data was a DSC822e commercialized by Mettler Toledo. The DSC results analysis for hydroquinone and d-mannitol are shown in Table 1.

Table 1. Materials selected as PCMs: melting temperature range and melting enthalpy obtained with DSC analysis.

Material	Formula	Melting temperature range [ºC]	Melting enthalpy [kJ/kg]
hydroquinone	$C_6H_6O_2$	165-172	235.2
d-mannitol (δ-phase)	$C_6H_{14}O_6$	155-162	260.8

Besides, the authors performed previous studies concerning the characterization of these materials and their performance at pilot plant scale [14,16-19]. The correct selection of materials to ensure the appropriate operation of the multiple PCM system is essential. For that, it is important to perform accurate laboratory tests regarding the enthalpy and melting and solidification temperature ranges.

2.2 Description of the pilot plant

The experimentation was performed at the pilot plant designed and built at the University of Lleida which allows experimentation with different storage systems and materials. This facility is mainly integrated by an electrical boiler of 24 kWe to heat the HTF up, acting as energy source during the charging process, and an air heat exchanger of 20 kWth to cool the HTF down

131 to simulate the real energy consumption. Synthetic thermal oil Therminol VP1 [20] was used as
132 HTF. Fig. 2 shows an overall view of the pilot plant above-described.
132

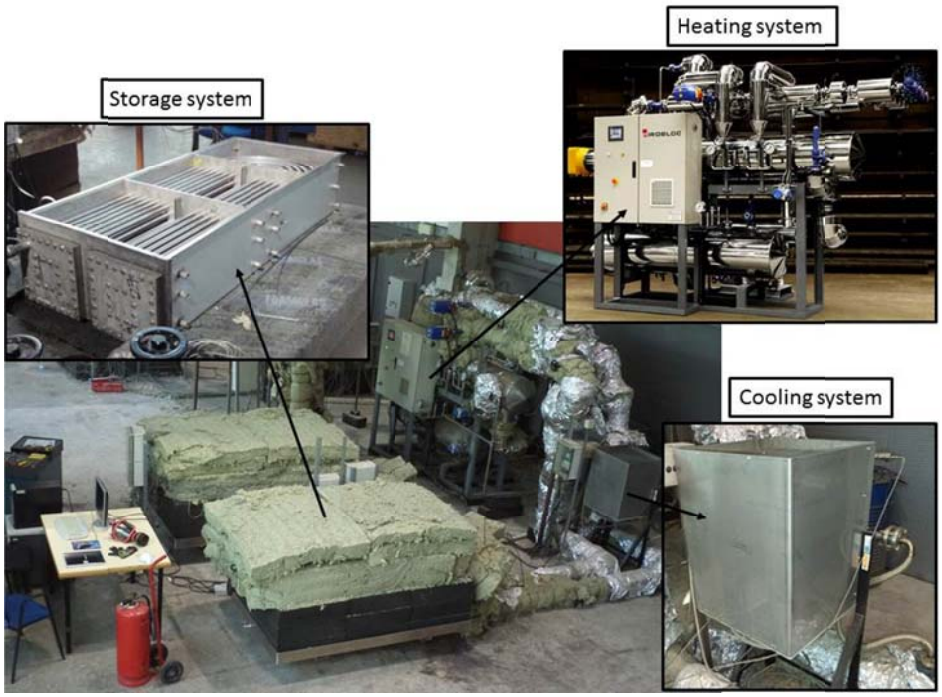

133
135 **Fig. 2. Overall view of the high temperature pilot plant used to perform the experimentation and its main**
136 **components.**
136

137 ### 2.3 Storage tanks

138

153 Two identical storage tanks made entirely of stainless steel, as shown in Fig. 3, were designed
154 and built at the University of Lleida to characterize at pilot plant scale different storage
155 materials. The design of the tanks was based on the concept of a shell-and-tubes heat exchanger
156 which consists on a vessel with a tubes bundle inside. The PCM was located in the housing of
157 the shell part and the HTF circulated inside the bundle of tubes, which was integrated for 49
158 tubes and distributed in square pitch. Table 2 shows the geometrical characteristics of the
159 storage tank used as well as the amount of PCM mass tested. 15 temperature sensors were
160 installed between the tubes bundle of the storage tank. Moreover, six temperature sensors in the
161 corners and six more in the center of the tank were installed for an accurate analysis of the PCM
162 thermal behavior, resulting in a total of 27 temperature sensors. When analyzing the temperature
163 behavior of the PCM inside the tank, it was stated that each temperature sensor would represent
164 a volume control and its influence would be weighted in relation to the amount of material in
165 this volume control. In order to be more representative, these temperature sensors are located at
166 different heights and at different depths of the tank. Four more temperature sensors were
167 installed in each storage tank to measure the inlet and outlet HTF temperatures. All the

temperature sensors were Pt-100 with an accuracy of 0.1 ºC. Furthermore, the HTF volume flow is measured during all the experimentation at the outlet of the electrical boiler using an orifice plate flow meter.

In order to easily understand the thermal behavior of the PCM inside the tank, the five temperature sensors located in the medium height have been chosen as the representative ones since their location inside the tanks aims to represent the evolution of the PCM along the HTF flow direction (T_2, T_5, T_8, T_{11} and T_{14} in Fig. 4).

Fig. 3. Overview of the TES tank pattern used to perform the experimentation.

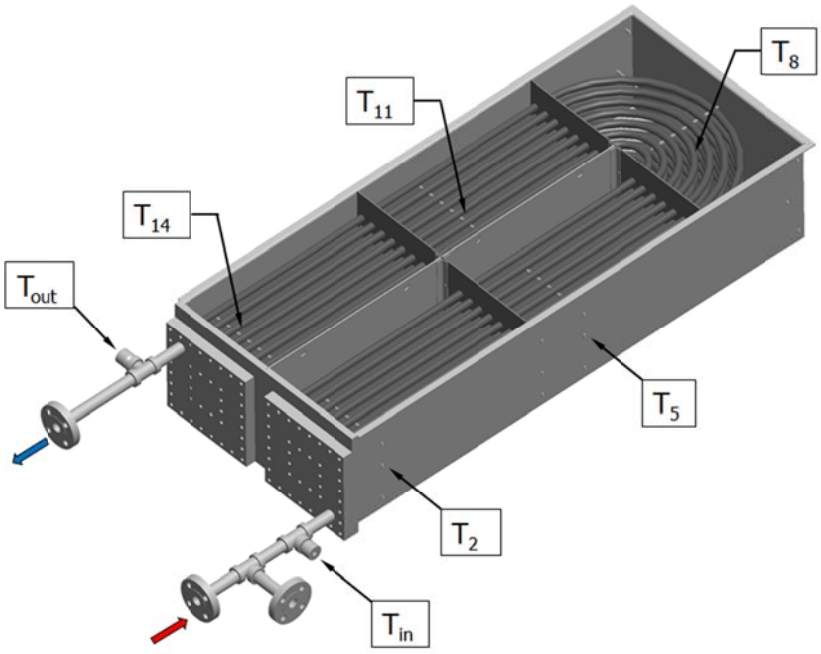

Fig. 4. Location of the seven temperature sensors used to calculate the thermal behaviour of the PCM (T_2, T_5, T_8, T_{11}, T_{14}) and the HTF (T_{in}, T_{out}).

With the purpose of minimizing the heat losses from the storage tank to the surroundings, 24 cm of rock wool were installed on the lateral walls and on the top of the storage tanks while 45 cm of Foamglass® were installed at the bottom.

Table 2. Geometrical characteristics of the TES tanks.

Characteristics	Value
Storage tank width [m]	0.527
Storage tank height [m]	0.273
Storage tank depth [m]	1.273
Tank vessel volume [m^3]	0.154
HTF pipes volume [m^3]	0.028
Number of HTF tubes [-]	49
HTF pipes thickness [m]	$2 \cdot 10^{-3}$
HTF pipes average length [m]	2.485
Heat transfer surface [m^2]	6.55
Total hydroquinone mass [kg]	170
Total d-mannitol mass [kg]	165

2.4 Methodology

Three different study cases are presented where the single PCM and the multiple PCMs configurations are compared during several charging processes and under the same thermal conditions (from Fig. 5 to Fig. 7). In this study, the multiple PCMs configuration is composed by two identical tanks connected in series but housing different PCM, for that, from now on the concept of twin configuration is included.

- Case 1: A single storage tank with a single PCM: hydroquinone, as shown in Fig. 5.

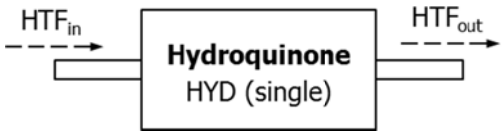

Fig. 5. Case 1, single PCM configuration (hydroquinone).

- Case 2: A single storage tank with a single PCM: d-mannitol, as shown in Fig. 6.

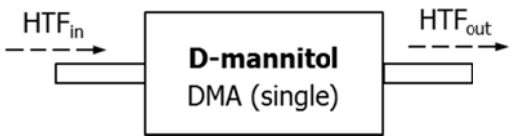

Fig. 6. Case 2, single PCM configuration (d-mannitol).

- Case 3: Two identical storage tanks with two different PCM arranged in series (twin configuration): hydroquinone and d-mannitol, as shown in Fig. 7. It can be observed that during the charging process, the HTF circulates first through the hydroquinone tank and then through the d-mannitol tank following the arrangement proposed in Fig. 1.

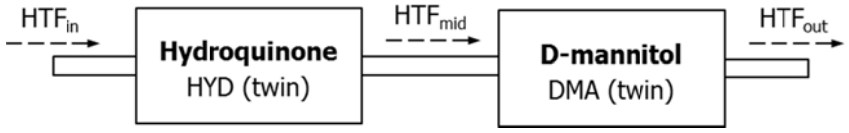

Fig. 7. Case 3, twin configuration (hydroquinone and d-mannitol).

In all three cases, the initial temperature of the PCM was set at 145 ºC and the HTF temperature was kept at 187 ºC during the charging process flowing at a flow rate of 2.8 m^3/h. These temperatures corresponded to the ones used in a real solar refrigeration application [14]. The charging process was considered to be finished once the difference of the HTF temperature and the average temperature of the PCM was 2 ºC. This difference takes into account the temperature oscillation of the heating system and the heating losses assumed in the system. In order to analyze the PCM behavior, the storage tanks have been divided into 27 control volumes where the PCM mass is known and temperature in each of them and measured by a temperature sensor. Despite the fact that several experiments were carried to ensure repeatability, only the most representative results are shown for better understanding.

The analysis of the advantages of using multiple (twin) PCMs configuration is done by studying the HTF and PCM temperature profiles over time and comparing the energy stored per mass unit (Eq. 1) as well as effectiveness (Eq. 2), since these two last parameters do not depend on the mass quantity in the tanks, which is different in the three cases presented.

The energy stored per mass unit, or specific energy, (e_{PCM}) considers the increase of enthalpy between the beginning (h_i) and the end (h_f) of the charging process. The enthalpy values are obtained through the DSC analysis with empirical equations as shown in Table 3.

$$e_{PCM} = \Delta h_{PCM} = h_f - h_i \qquad \text{Eq. 1}$$

Table 3. Enthalpy empirical equations used to calculate the energy stored by both the hydroquinone and d-mannitol

Material	Sensible	Latent	Sensible

	phase (s)	phase	phase (l)
hydroquinone	h(T) = 2.128·T – 298.33	h(T) = 8.393·T^2 – 2800.2·T + 233618	h(T) = 2.644·T – 167.51
d-mannitol (δ-phase)	h(T) = 3.208·T – 452.19	h(T) = 6.173·T^2 – 1987.9·T + 160114	h(T) =4 .517·T – 411.32

Effectiveness parameter, introduced by Belusko and Bruno [21] is described as the ratio of the actual heat discharged ($\dot{Q}_{experiment}$) over the theoretical maximum heat that can be discharged ($\dot{Q}_{theoric}$). This parameter is only calculated in the phase change temperature range (Eq. 2).

$$\varepsilon = \frac{\dot{Q}_{experiment}}{\dot{Q}_{theoric}} = \frac{(T_{HTF\,in} - T_{HTF\,out})}{(T_{HTF\,in} - T_{PCM\,.m})} \quad \text{Eq. 2}$$

Where T_{HTFin} is the inlet HTF temperature, $T_{HTF\,out}$ is the outlet HTF temperature and $T_{PCM\,.m}$ is the average melting temperature of the PCM.

In Case 3, during both the latent and the sensible phase in the liquid region, the overall thermal resistance between the HTF and the PCM has been determined by implementing a mathematical model similar to the one developed by Gil et al. [22] as Fig. 8 shows. This model allowed the authors to obtain the effective thermal conductivity (Eq. 3) of both hydroquinone and d-mannitol and therefore to study the influence of the convection together with the conduction in the behavior of the material in the twin configuration.

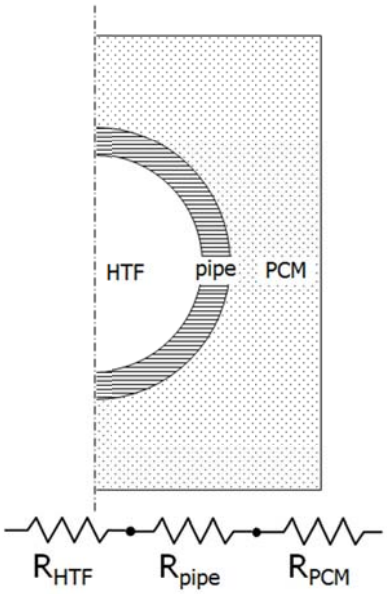

Fig. 8. Thermal resistance model of the studied system.

The following assumptions were introduced to simplify the mathematical model:

- The model is simplified to one tube and the PCM influenced by it.
- Thermopyhisical properties remain constant during the melting process.
- For the HTF side: the flow is hydrodinamically developed. During the melting process the fluid is considered to flow under steady state
- For the pipe side: the temperature of the pipe is considered constant along the pipe and equal to the average value between the inlet and the outlet HTF temperature.
- For the PCM side: adiabatic boundary conditions. Reference temperature at T_{PCM8}. During the melting process, the temperature was considered as the average value of the temperature melting range and the natural convection was considered as well.

$$k_{eff} = \frac{1}{R_{PCM} \cdot S} \quad \text{Eq. 3}$$

Where R_{PCM} is the thermal resistance of the PCM and S is the shape factor of the present model. Solving Eq. 4 for the thermal resistance of the PCM leads to:

$$R_{PCM} = R_t - R_{HTF} - R_p \quad \text{Eq. 4}$$

Where R_t, R_{HTF} and R_p are the thermal resistances of the system, HTF and pipe respectively.

The thermal resistance of the system (R_t) is calculated according to Eq. 5:

$$R_t = \frac{1}{U \cdot A} \quad \text{Eq. 5}$$

Assuming the storage tank as a heat exchanger, then the value of $U \cdot A$ can be calculated by isolating it from the equation used to obtain the power transferred from the HTF to the PCM (Eq. 6). It shows the power absorbed by the PCM ($\dot{Q}_{PCM}$), which is calculated with an energy balance between the above-mentioned PCM absorbed power, the power released by the HTF, the losses to the environment and the accumulated energy in both the HTF and metal parts of the tank.

$$\dot{Q}_{PCM} = U \cdot A \cdot \Delta T_{LMTD} \quad \text{Eq. 6}$$

On the other hand, the logarithmic mean temperature difference (ΔT_{LMTD}) is calculated as shown in Eq. 7:

$$\Delta T_{LMTD} = \frac{(T_{HTFin} - T_{PCM.m}) - (T_{HTFout} - T_{PCM.m})}{\ln\left(\frac{T_{HTFin} - T_{PCM.m}}{T_{HTFout} - T_{PCM.m}}\right)} \quad \text{Eq. 7}$$

The thermal resistance of the pipe (R_p) is calculated according to Eq. 8:

$$R_p = \frac{1}{2 \cdot \pi \cdot L \cdot k_p} \cdot \ln\left(\frac{D_{ext}}{D_{int}}\right) \quad \text{Eq. 8}$$

The thermal resistance of the HTF (R_{HTF}) is calculated taking into account the forced convection in a pipe with internal flow according to Eq. 9:

$$R_{HTF} = \frac{1}{\alpha_{HTF} \cdot A_{int}} = \frac{1}{\frac{Nu \cdot k_{HTF}}{D_{int}} \cdot \pi \cdot D_{int} \cdot L} \quad \text{Eq. 9}$$

Where the thermal conductivity of the HTF (k_{HTF}) was obtained with the data provided by the manufacturer and the Nusselt number (Nu) is obtained with the correlation provided by Sieder and Tate [23] an presented in Eq. 10 in case the Reynolds number showed laminar flow and with the Gnielinski correlation [24] and presented in Eq. 11 in case the Reynolds number showed turbulent flow.

$$Nu_{Re \leq 2300} = 1.86 \cdot Re^{1/3} \cdot Pr^{1/3} \cdot \left(\frac{\mu_b}{\mu_w}\right)^{0.14} \cdot \left(\frac{D_{int}}{L}\right)^{1/3} \quad \text{Eq. 10}$$

$$Nu_{Re \geq 2300} = \frac{(Re - 1000) \cdot Pr \cdot \left(\frac{f}{8}\right)}{1 + 12.7 \cdot (Pr^{2/3} - 1) \cdot \left(\frac{f}{8}\right)^{1/2}} \quad \text{Eq. 11}$$

For a fully developed turbulent flow, the correlation which approximates the friction factor (f) was developed by Petukhov [25] and is of the form that Eq. 12 shows:

$$f = \frac{1}{(0.79 \cdot \ln(Re) - 1.64)^2} \quad \text{Eq. 12}$$

On the other hand, the shape factor (S) is calculated as Eq. 13 shows and taking into account the parameters described in Fig. 9 and Table 4.

$$S = \frac{2 \cdot \pi \cdot L}{\ln\left(1.08 \cdot \frac{W}{D_{ext}}\right)} \quad \text{Eq. 13}$$

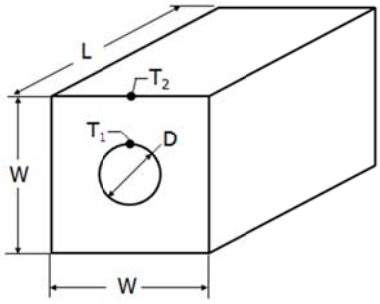

Fig. 9. Shape factor of the simplified model of the tank. Adapted from [26].

Table 4. Storage tank characteristics to calculate the shape factor parameter.

Parameter	Value	Units
L	2900	mm
W	31	mm
D_{ext}	19	mm
T_1	$(T_{HTFin} + T_{HTFout})/2$	ºC
T_2	$T_{PCM.8}$	ºC

3. Results and discussion

Heat transfer rate depends directly on the difference between the inlet and outlet HTF temperatures. For that, Fig. 10 shows the outlet HTF temperatures during the charging process of the three different cases studied. As expected, the outlet HTF temperature of Case 1 and Case 2, which corresponds to the single tank configuration with hydroquinone and d-mannitol respectively, has almost the same values, being the temperature from the Case 2 slightly higher due to their thermophysical properties. Furthermore it can be seen that the temperature of these two cases rapidly increases to values close to the inlet temperature during the first hour of experimentation and afterwards the increase becomes more moderate. On the other hand, the outlet HTF temperature of the Case 3, which corresponds to the twin configuration, has lower and more uniform values than the previous two cases during all the experimentation. The larger the temperature difference between the inlet and outlet HTF temperatures, the higher the heat transfer rate. As a result, an increasing in a factor of 4 could be achieved in the average heat transfer rate by implementing the multiple PCM storage configuration.

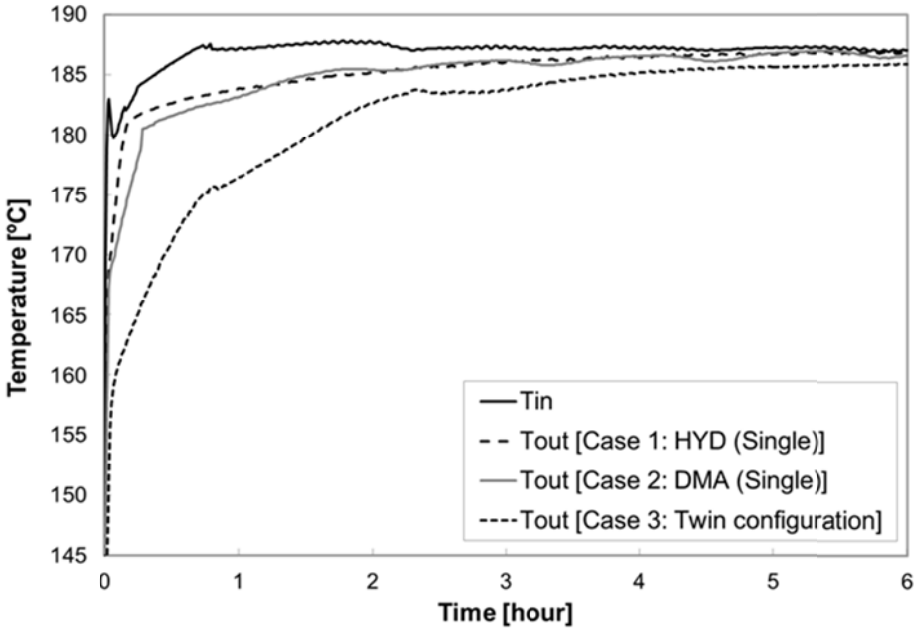

Fig. 10. HTF temperature profiles in the three cases studied.

Fig. 11 shows the energy stored per unit mass, or specific energy, during the charging process in the three different cases studied. Notice that Case 3 is split in three different studies in order to show both the behavior of the whole system, Twin configuration, and the behavior of the two different tanks within the twin configuration, HYD (Twin) and DMA (Twin). As it can be seen, Case 1 showed the lowest value of specific energy stored, with a value close to 0.09 kWh/kg. It is an expected behavior since hydroquinone has an enthalpy value lower than d-mannitol. Taking into account the total amount of mass of hydroquinone, the tank stores a total of 15.3 kWh at the end of the charging process. On the other hand, Case 2 shows the highest and fastest response in the specific energy because of the highest enthalpy and temperature difference, with a value close to 0.115 kWh/kg. Moreover, taking into account the total amount of mass of d-mannitol, the tank stores a total amount of 18.5 kWh at the end of the charging process. When considering Case 3 as the whole twin configuration, the energy accumulated values through time get intermediate values between the d-mannitol and the hydroquinone tanks, as expected. On the other hand, if a tank by tank evaluation in the twin configuration is considered, it can be observed that from 1:20 h on, which corresponds to the final stage of the melting process, the tank shows the same behavior than the single PCM configuration tanks.

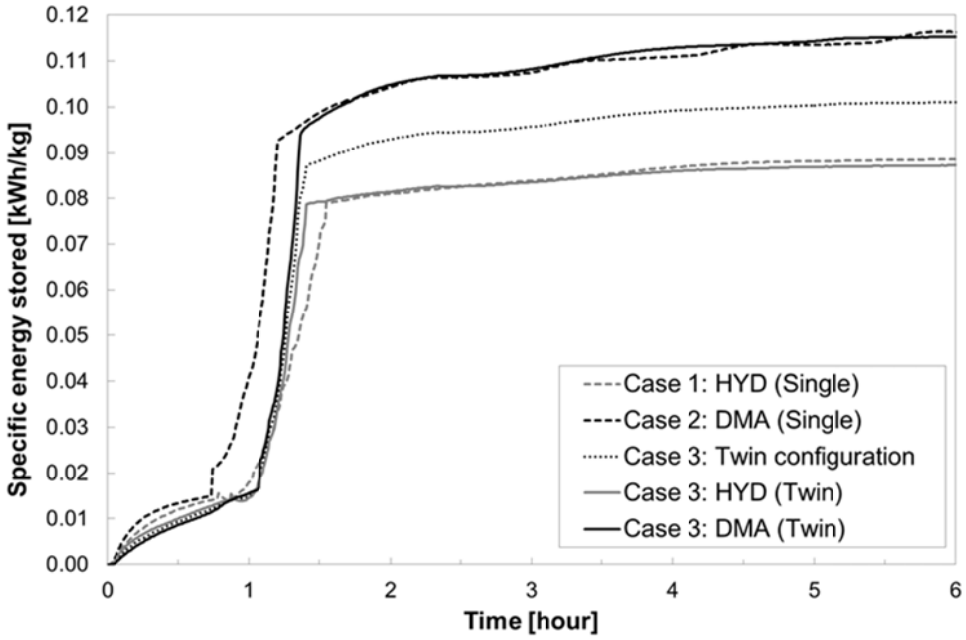

339
340 **Fig. 11. Energy stored per unit mass in the three cases studied over the experimentation.**
341

354 In Fig. 12 the evolution of the effectiveness over the melting process period is shown in order to
355 study, tank by tank, if any benefit is observed by implementing the twin configuration. A
356 decreasing trend over time on the effectiveness parameter can be seen. It is an expected
357 behavior since effectiveness depends on a temperature difference (Eq. 2). Furthermore, if
358 hydroquinone is taken into account, a very similar effectiveness performance can be seen in
359 both the single tank configuration and the twin PCMs configuration. The reason is because in
360 both configurations there are the same working conditions (material and inlet HTF temperature)
361 and therefore the outlet HTF temperature is practically the same and the only differences,
362 mostly at the beginning of the melting process, are mainly due to human manipulation and
363 ambient conditions. On the other hand, if d-mannitol is taken into account, an average
364 effectiveness enhancement of 19.36% could be achieved in the twin configuration if compared
365 to the single PCM configuration, which is mainly due to the higher uniformity on the HTF
366 outlet temperature.
355

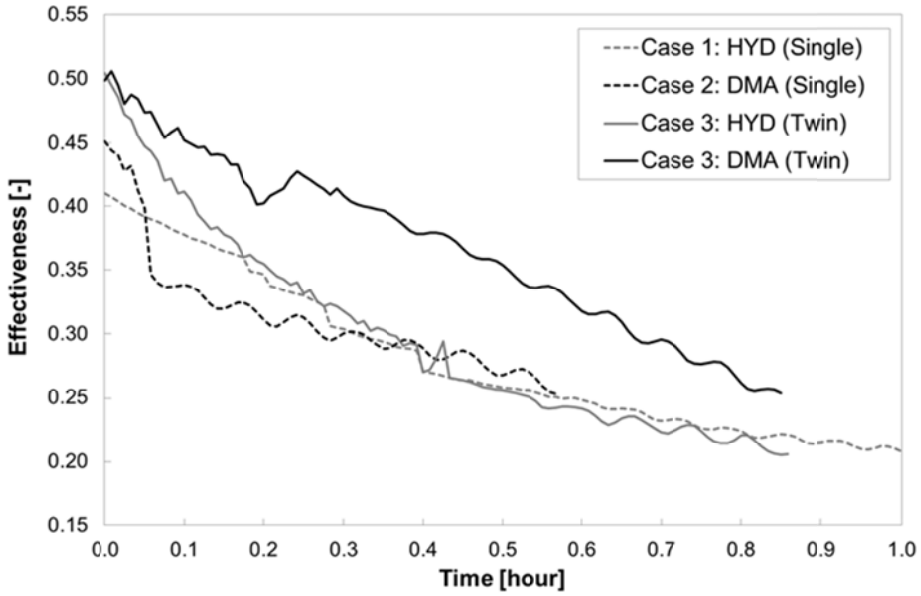

Fig. 12. Evolution of the effectiveness in the hydroquinone and d-mannitol tanks in both the multiple PCMs and single configuration during the melting process.

If focusing on the twin configuration (Case 3), the HTF and PCM temperature profiles are shown in Fig. 13 and Fig. 14. First, Fig. 13 shows the HTF temperature at eight different intervals of time, from the beginning to the end of the charging process, in three different locations: inlet of the first tank ($T_{HTF\ in}$), between the first and second tank ($T_{HTF\ mid}$), and at the outlet of the second tank ($T_{HTF\ out}$). The inlet HTF temperature is constant at a value of 187 ºC and both the middle and outlet HTF temperature have a progressive increase over the time until both temperatures have practically the same value. As expected, this increase is accentuated since a bigger amount of heat is transferred and as the experimentation goes by this temperature difference decreases progressively until the temperatures of both tanks are practically the same.

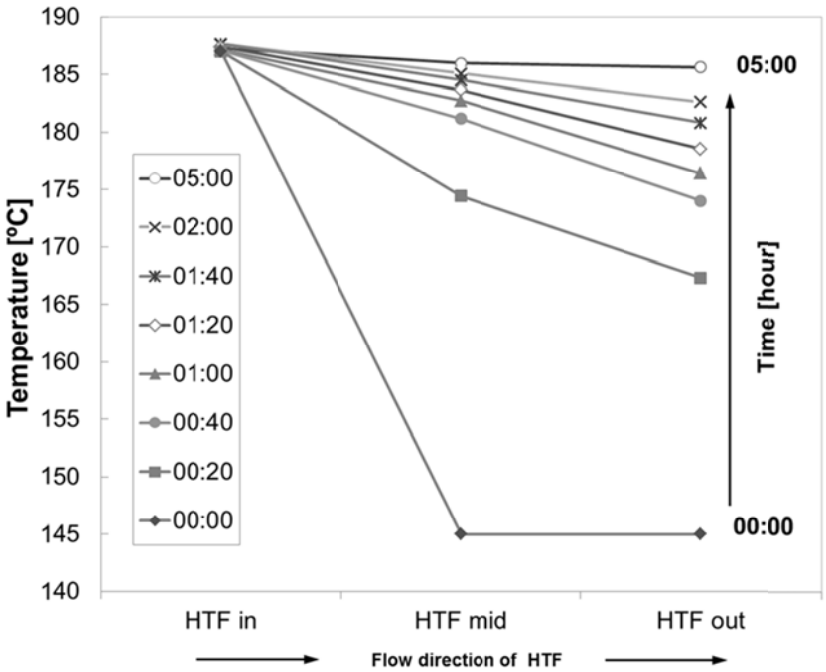

Fig. 13. Case 3: HTF temperature over the experimentation in the inlet of the first tank (HTF_{in}), between the first and second tank (HTF_{mid}), and at the outlet of the second tank (HTF_{out}).

Fig. 14 shows the PCM temperature profile of the above-mentioned five representative sensors (Fig. 4) over time in both storage tanks during the charging process. Moreover, melting temperature ranges from both PCMs are highlighted in grey for better visual understanding. During the sensible heating part in the solid region, the temperature sensors located close to the inlet of the first tank (T_{HTFin}) increase faster their temperature than the rest, as expected. However, temperature sensors $T_{PCM.11}$ and $T_{PCM.14}$ in the first tank do not show the expected tendency due to the high influence of the thermal conduction from the control volumes monitored by $T_{PCM.2}$ and $T_{PCM.5}$ because of the pipe bundle U shape (Fig. 3). Regarding the latent phase, it can be seen that hydroquinone starts melting after 30 minutes from the beginning of the charging process and it is completely melted after 1:40 h. Analogously, d-mannitol starts the melting process faster than the hydroquinone, after 20 minutes from the beginning, and it is completely melted after 1:20 h. During this process, a better uniformity in both materials is observed but d-mannitol temperature sensors start to show values higher than hydroquinone, situation which is even increased during the sensible heating part in the liquid region, despite the fact that hydroquinone is set in the upstream of HTF and the d-mannitol is in the downstream. This is mainly due to the fact that d-mannitol has the melting temperature range lower than hydroquinone and while some regions of the first tank are still under phase change, some other regions of the second tank have already changed of phase and are able to increase temperature faster because of the higher temperature difference between PCM and HTF.

Results from the mathematical model showed that the effective thermal conductivity of d-mannitol during the melting process was 34.7 % higher than the effective thermal conductivity of hydroquinone, and during the sensible phase in the liquid region, this difference was even more highlighted, being the effective thermal conductivity of d-mannitol 207.2 % higher. These results, together with a higher temperature difference between the PCM and the HTF explain why during the liquid region the material in the second tank of the twin configuration shows higher temperatures than the first.

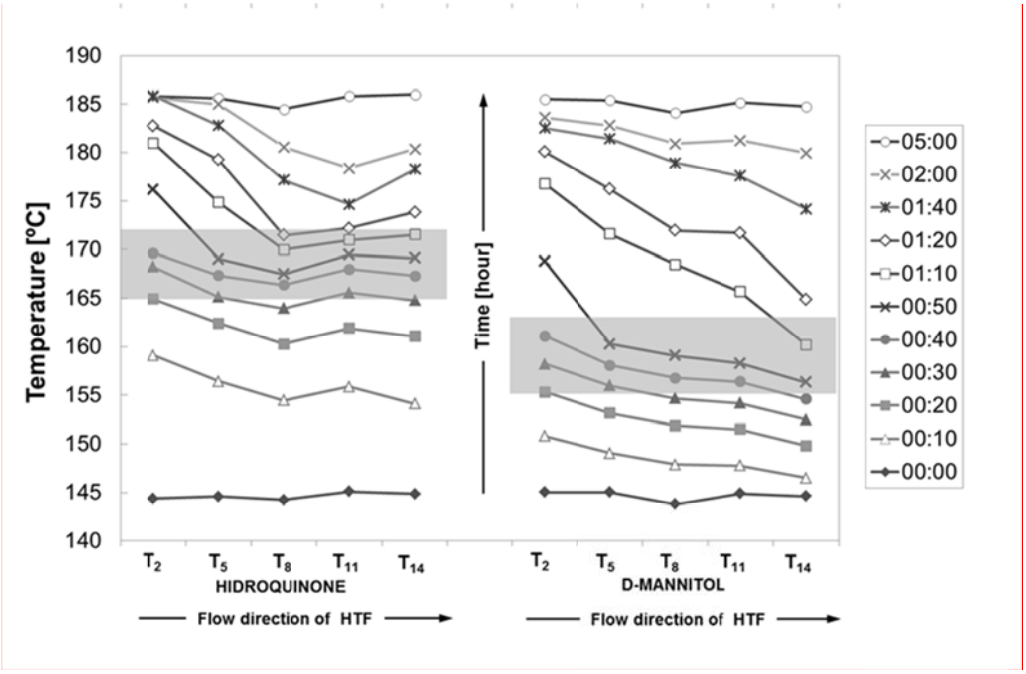

Fig. 14. Case 3: Temperature of both PCM over the experimentation.

4. Conclusions

In the present paper, the advantages of using the multiple PCMs configuration instead of the single PCM configuration in TES systems are experimentally analyzed at pilot plant scale. In the literature, few papers study the multiple PCMs concept and among them, any experimentally evaluated such concept at medium-high scale. Therefore, two PCMs with melting temperatures between 150-200 ºC and with high values of heat of fusion, hydroquinone and d-mannitol, are experimentally analyzed in the pilot plant facility of the University of Lleida. Three different cases are studied: (1) single PCM configuration with hydroquinone, (2) single PCM configuration with d-mannitol, and (3) multiple PCMs configuration with hydroquinone and d-mannitol. The energy stored per unit mass, effectiveness and HTF temperature profile during the charging process are calculated and analyzed in the three cases. For a better comprehension

of the multiple PCMs configuration, HTF and PCM temperatures profiles in an exhaustive way are studied. Results showed that the multiple PCMs configuration introduces a higher uniformity on the HTF temperature difference between the inlet and outlet and, as a consequence, higher heat transfer rates during a higher period can be achieved. Moreover, in terms of effectiveness, an average enhancement of 19.36 % in comparison with the single PCM configuration can also be obtained.

Acknowledgements

The work is partially funded by the Spanish government (ENE2011-22722 and ULLE10-4E-1305). The authors would like to thank the Catalan Government for the quality accreditation given to their research group GREA (2014 SGR 123). The research leading to these results has received funding from the European Union's Seventh Framework Programme (FP7/2007-2013) under grant agreement n° PIRSES-GA-2013-610692 (INNOSTORAGE). Laia Miró would like to thank the Spanish Government for her research fellowship (BES-2012-051861). The authors would like to thank Dr. Eduard Oró from Catalonia Institute for Energy Research (Spain) and Dr. Antoni Gil from Massachusetts Institute of Technology (USA) for their help during the initial stages of the experimentation design.

References

[1] International Energy Agency. Int Energy Agency n.d. http://www.iea.org (accessed November 17, 2014).

[2] Domański R, Fellah G. Exergy analysis for the evaluation of a thermal storage system employing PCMS with different mlting temperatures. Appl Therm Eng 1996;16:907–19. doi:10.1016/1359-4311(96)00003-8.

[3] Seeniraj RV, Lakshmi Narasimhan N. Performance enhancement of a solar dynamic LHTS module having both fins and multiple PCMs. Sol Energy 2008;82:535–42. doi:10.1016/j.solener.2007.11.001.

[4] Wang J, Ouyang Y, Chen G. Experimental study on charging processes of a cylindrical heat storage employing multiple-phase-change materials. Int J Energy Res 2001;25:439–47. doi:10.1002/er.695.

[5] Tian Y, Zhao CY. Thermal and exergetic analysis of Metal Foam-enhanced Cascaded Thermal Energy Storage (MF-CTES). Int J Heat Mass Transf 2013;58:86–96. doi:10.1016/j.ijheatmasstransfer.2012.11.034.

[6] Jegadheeswaran S, Pohekar SD. Performance enhancement in latent heat thermal storage system: A review. Renew Sustain Energy Rev 2009;13:2225–44. doi:10.1016/j.rser.2009.06.024.

[7] Farid MM, Kanzawa A. Thermal performance of a heat storage module using PCM's with different melting temperatures: Mathematical modeling. J Sol Energy Eng Trans ASME 1989;111:152–7.

[8] Farid MM, Kim Y, Kansawa A. Thermal performance of a heat storage module using PCM's with different melting temperature: experimental. J Sol Energy Eng Trans ASME 1990;112:125–7.

[9] Cui H, Yuan X, Hou X. Thermal performance analysis for a heat receiver using multiple phase change materials. Appl Therm Eng 2003;23:2353–61. doi:10.1016/S1359-4311(03)00210-2.

[10] Gong ZX, Mujumdar AS. New solar receiver thermal store for space-based activities using multiple composite phase-change materials. J Sol Energy Eng Trans ASME 1995;117:215–20.

[11] Michels H, Pitz-Paal R. Cascaded latent heat storage for parabolic trough solar power plants. Sol Energy 2007;81:829–37. doi:10.1016/j.solener.2006.09.008.

[12] Chiu JNW, Martin V. Multistage latent heat cold thermal energy storage design analysis. Appl Energy 2013;112:1438–45. doi:10.1016/j.apenergy.2013.01.054.

[13] Shabgard H, Robak CW, Bergman TL, Faghri A. Heat transfer and exergy analysis of cascaded latent heat storage with gravity-assisted heat pipes for concentrating solar power applications. Sol Energy 2012;86:816–30. doi:10.1016/j.solener.2011.12.008.

[14] Gil A, Oró E, Castell A, Cabeza LF. Experimental analysis of the effectiveness of a high temperature thermal storage tank for solar cooling applications. Appl Therm Eng 2013;54:521–7. doi:10.1016/j.applthermaleng.2013.02.016.

[15] Brückner S, Liu S, Miró L, Radspieler M, Cabeza LF, Lävemann E. Industrial waste heat recovery technologies: An economic analyisis of heat tranformation technologies. Accepted in Applied Energy n.d.

[16] Gil A, Oró E, Peiró G, Álvarez S, Cabeza LF. Material selection and testing for thermal energy storage in solar cooling. Renew Energy 2013;57:366–71. doi:10.1016/j.renene.2013.02.008.

[17] Gil A, Oró E, Miró L, Peiró G, Ruiz Á, Salmerón JM. Experimental analysis of hydroquinone used as phase change material (PCM) to be applied in solar cooling refrigeration. Int J Refrig 2014;39:95–103. doi:10.1016/j.ijrefrig.2013.05.013.

[18] Oró E, Gil A, Miró L, Peiró G, Álvarez S, Cabeza LF. Thermal energy storage implementation using phase change materials for solar cooling and refrigeration applications. vol. 30, 2012, p. 947–56. doi:10.1016/j.egypro.2012.11.107.

[19] Barreneche C, Gil A, Sheth F, Inés Fernández A, Cabeza LF. Effect of d-mannitol polymorphism in its thermal energy storage capacity when it is used as PCM. Sol Energy 2013;94:344–51. doi:10.1016/j.solener.2013.05.023.

[20] Therminol VP-1 product information. http://www.therminol.com/products/Therminol-VP1 (accessed January 7, 2015).

[21] Belusko M, Bruno F. Design methodology of PCM thermal storage systems with parallel plates. EuroSun Conf. 2008, Lisbon, Portugal: 2008.

[22] Gil A, Oró E, Salmerón JM, Cabeza, LF, Álvarez S. Experimental analysis of the effective thermal conductivity enhancement of PCM using finned tubes in high temperature bulk tanks. Innostock 2012. The 12th International Conference on Energy Storage.

[23] Sieder EN, Tate GE. Heat Transfer and Pressure Drop of Liquids in Tubes,. Eng Chem 1936;28:1429–36.

[24] Gnielinski V. New equations for heat and mass transfer in turbulent pipe and channel flow. Forschung im Ingenieurwesen 1975;41: 8–16.

[25] Petukliov BS. Heat transfer and friction in turbulent pipe flow with variable physical properties, Advances in Heat Transfer 1970; 6.

[26] Nellis G, Klein S. Heat transfer. 1st ed. New York: Cambridge University Press; 2009.